Search for Postinflationary QCD Axions with a Quantum-Limited Tunable Microwave Receiver

G. Sardo Infirri,[1,2,*] D. Alesini,[3] C. Braggio,[1,2] G. Cappelli,[4] G. Carugno,[1,2] D. D'Agostino,[5] A. D'Elia,[3] D. Di Gioacchino,[3] R. Di Vora,[6] M. Esposito,[4,†] P. Falferi,[7,8] U. Gambardella,[5] A. Gardikiotis,[1] C. Gatti,[3] C. Ligi,[3] G. Lilli,[6] A. Lombardi,[6] G. Maccarrone,[3] D. Maiello,[1,2] A. Ortolan,[6] A. Ranadive,[4,‡] A. Rettaroli,[3] N. Roch,[4] S. Tocci,[3] and G. Ruoso[6,§]

(QUAX Collaboration)

[1]*INFN, Sezione di Padova, 35100 Padova, Italy*
[2]*Dipartimento di Fisica e Astronomia, Università degli Studi di Padova, 35100 Padova, Italy*
[3]*INFN, Laboratori Nazionali di Frascati, 00044 Frascati, Roma, Italy*
[4]*Université Grenoble Alpes, CNRS, Grenoble INP, Institut Néel, 38000 Grenoble, France*
[5]*INFN, Sezione di Napoli, 80126 Napoli, Italy*
[6]*INFN, Laboratori Nazionali di Legnaro, 35020 Legnaro, Padova, Italy*
[7]*Istituto di Fotonica e Nanotecnologie, CNR Fondazione Bruno Kessler, 38123 Povo, Trento, Italy*
[8]*INFN, TIFPA, 38123 Povo, Trento, Italy*

(Received 16 June 2025; accepted 8 October 2025; published 19 November 2025)

A search for cosmological axions has been performed by scanning a frequency region of 38 MHz centered at about 10.2 GHz, corresponding to an axion mass $m_a \simeq 42$ μeV. The QUAX experimental apparatus, a haloscope comprised of a 1-liter volume tunable cavity immersed in an 8 T magnetic field and a quantum-limited detection chain, set limits on the axion-photon coupling at the 10^{-14} GeV^{-1} level. As no signal candidate has been observed, viable hadronic axion models are ruled out in a currently preferred postinflationary region $m_a > 40$ μeV.

DOI: 10.1103/4dv9-72t5

Introduction—The axion was introduced to solve the strong *CP* problem, i.e., the absence of *CP* violation in quantum chromodynamics (QCD). Solution to the strong *CP* problem came with the new symmetry called Peccei Quinn (PQ), of which the axion is the pseudo Goldstone boson [1–3]. The axion soon became a well-motivated dark matter candidate [4–6], but its mass is still unknown and the possible value ranges over several decades [7]. Axion couplings to ordinary matter depend on the specific model used to incorporate the PQ symmetry into an extension of the standard model of particle physics. The two most popular classes of models are known as KSVZ [8,9] and DFSZ [10,11]. A detailed description of their extended parameter space can be found in [12]. With the assumption that all the local dark matter density is saturated by axions, a few experimental searches have been able to probe the specific axion-photon coupling predicted by such models. The most sensitive probes are called haloscopes and are based on tunable resonant cavities immersed in a strong magnetic field [13,14]. Provided the axion energy matches the haloscope cavity resonance frequency, conversion of dark matter axions to photons is resonantly enhanced by the cavity quality factor, resulting in a higher sensitivity [15,16]. In the axion mass region below 30 μeV, only ADMX [17] and CAPP [18] experiments reached DFSZ sensitivity while HAYSTAC [19] achieved near-KSVZ sensitivity. Searches at higher masses are flawed by unfavorable scaling of the cavity haloscope experimental parameters. Recently, dish antenna [20], dielectric haloscopes [21], and plasma haloscopes [22] were introduced to tackle higher masses; however, the sensitivity of these instruments is still limited.

Recent works based on lattice simulations [23,24] motivate the search for postinflationary axions [25] with masses above 40 μeV. In this mass region no extended

*Contact author: Giosue.Sardo@pd.infn.it
†Present address: CNR-SPIN Complesso di Monte S. Angelo, via Cintia, Napoli, 80126, Italy.
‡Present address: Google Quantum AI, Goleta California 93117, USA.
§Contact author: Giuseppe.Ruoso@lnl.infn.it

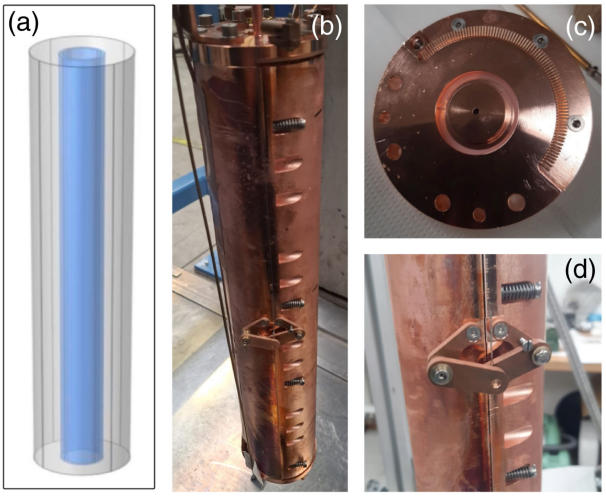

FIG. 1. (a) The microwave resonator is a dielectrically loaded cylindrical cavity. The main structure is a copper cylinder with length 414.3 mm and 60.5 mm diameter (gray area). The cylinder is longitudinally cut in two halves and can be opened with a clamshell-like movement for tuning. It includes a 420 mm long sapphire tube with 21.8 mm inner diameter and 30.2 mm outer diameter (blue area). The sapphire cylinder extends into the cavity end caps by 5.3 mm deep annular grooves. (b) A picture of the cavity mounted in the dilution refrigerator is also shown. (c) End cap with annular grooves for holding the sapphire and springs for keeping the rf contact while tuning. (d) Pantograph for tuning.

searches have yet been conducted at QCD axion sensitivity, required to probe the KSVZ or DFSZ classes of models.

The experiment QUaerere AXion (QUAX) has been conceived to search for axion dark matter in the $35-45$ μeV mass window, corresponding to the frequency range from 8.5 to 11 GHz. It is built around two complementary cavity haloscopes covering two distinct mass regions. The QUAX haloscope located in the Laboratori Nazionali di Frascati of INFN is designed to work in the lower half of the proposed mass range, and a pilot measurement has been recently performed at a mass of $\simeq 26.5$ μeV [26]. The QUAX haloscope operating at the Laboratori Nazionali di Legnaro targets instead axion searches above 10 GHz. It has already conducted several test runs, obtaining near KSVZ model sensitivity in a region above 40 μeV [27–30].

In this Letter results are reported of a cosmological axion search using the improved high frequency QUAX haloscope. The novel version of the apparatus allows for frequency tuning of the resonant detection system with uniform axion sensitivity over a broad range. For the longest single acquisitions an axion sensitivity at about the KSVZ model is reached, while the typical sensitivity allows us to probe axion-photon coupling values predicted within the hadronic QCD axion models [12].

Experimental apparatus and data collection—The experimental setup is an evolution of the one presented in Ref. [30]. To allow for a wider frequency tuning, a new dielectrically loaded cavity has been developed, in which a large effective volume is obtained by inserting a sapphire cylinder in a right cylindrical copper cavity and selecting the TM030 as the science mode (see Fig. 1). The copper cylinder is divided into two halves to allow for changing the frequency by a clamshell mechanism detailed in Ref. [31], where a similar cavity working at about 11 GHz has been studied. The tuning mechanism opens the two halves with a panthographlike system. It is actuated via a 100 μm diameter wire, pulled remotely by a room-temperature motor. The correct working is ensured by restoring springs, which act as counterbalance. The design prioritizes operational reliability by means of a mechanical stop to limit the lever travel: it prevents the mechanism from passing a nonreturn point at the cost of a constrained tuning. The resulting range, with a one degree aperture angle, is $10.212-10.154$ GHz. Solutions for an increased tuning range are currently foreseen.

Detailed mode reconstruction is performed with finite element simulations to calculate the cavity form factor C_{030} [32], which measures the coupling of the axion field to the specific cavity mode for different aperture. Simulations give $C_{030}=0.43$, which complies with the room temperature bead pull measurement [33] giving $C_{030}=0.40\pm0.02$. This latter result is obtained with a cavity opening angle of about 0.3°. Following results from simulations, this value is assumed to be constant throughout the frequency tuning region.

The apparatus lies inside the science chamber of a wet dilution refrigerator (DR), with the cavity kept at about 100 mK (see [30] for details). During data acquisition, the liquid helium level is monitored, and refills take place every 24 h, thus ensuring good thermal stability of the system. The cavity temperature is stable within a few mK, after a few days necessary for thermalization. Temperature stability also ensures gain stability for the detection chain.

The detection chain is largely similar to what is described in Ref. [30], with a traveling wave parametric amplifier (TWPA) [34] used as a first stage amplifier. The TWPA, kept at about 120 mK, is followed by a cryogenic high electron mobility transistor (HEMT) amplifier placed in the 4 K stage of the DR, and then by another HEMT at room temperature.

The output of the room temperature HEMT is down-converted with a carrier frequency f_{LO} shifted by 1 MHz from the cavity frequency f_c. In-phase and quadrature products are amplified, low-pass filtered to avoid aliasing and sampled with an analog to digital converter working at the frequency of 4.4 MS/s. Every 2^{23} samples, i.e., about 1.9 s, data are stored in a file; in a typical acquisition step, 2000 data blocks of this length are acquired.

Two run sessions have been performed, the first in June 2024 and the second in November 2024. The integrated acquisition time is about 225 h, distributed over 18 days, with a resulting data collection efficiency of about 50%. Residual time is mainly used for cavity tuning,

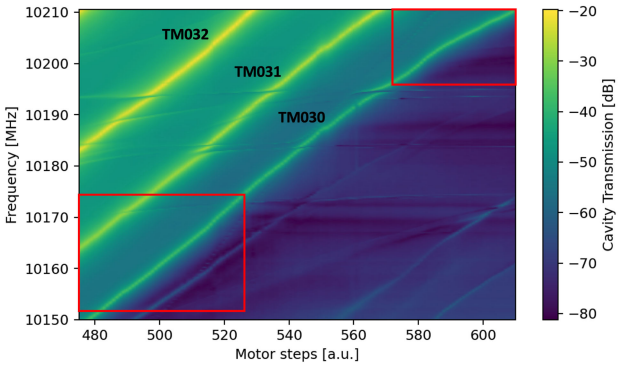

FIG. 2. Cavity mode map showing the lowest order TM03n modes versus steps of the motor used for tuning. Science mode is the TM030, which can be tuned up to 10.212 GHz. Because of nonlinearities in the actuation system, there is no strict linear relation between steps and frequency change. The studied frequency ranges are enclosed in the red boxes. It is also evident of the presence of intruder modes in the region 10.180–10.196 GHz.

optimization of the TWPA performance, and measurement of the working parameters: cavity resonance frequency and quality factor, antenna coupling, receiver gain profile and noise temperature at the cavity peak frequency. Data acquisition is partially automated: while cavity tuning and amplifier optimization is still performed by the operator, all other measurements are controlled by the data acquisition software.

Axion searches have been performed in a measurement window of about 38 MHz, corresponding to about 65% of the available tuning range. The presence of intruder modes (see Fig. 2) degrading the system performance is the main reason for the reduced range, together with a mechanical problem in the tuning mechanism that precluded a fine tuning in the interval 10.175–10.196 GHz. Tuning was performed using a step size of approximatively one cavity linewidth. Only for a few measurement points, steps close to two cavity linewidths have been chosen. The total number of measurement points P_m was 124.

Figure 3(a) shows the measured values of the cavity unloaded quality factor at each frequency tuning step. Pick-up antenna coupling, set to an initial value of $\beta = 1.6$ and never optimized during the run, was measured to vary approximately from 1.5 to 1.8. An enhanced spreading of quality factor and antenna coupling values was caused by mechanical clearances in the positioning of the cavity elements at each step. The value of β was chosen to have near-to-optimum scan rate, where the optimal value for scanning is $\beta = 2$. Conversely, $\beta \simeq 1.1$ was used to increase axion sensitivity in some measurement points at the cost of a slower scan rate.

System noise temperature $T_{\rm sys}$ is measured at each point P_m using the procedure described in [35], improved compared to past versions thanks to a computer controlled system acting on a number of rf switches. A single measurement of system noise temperature requires about

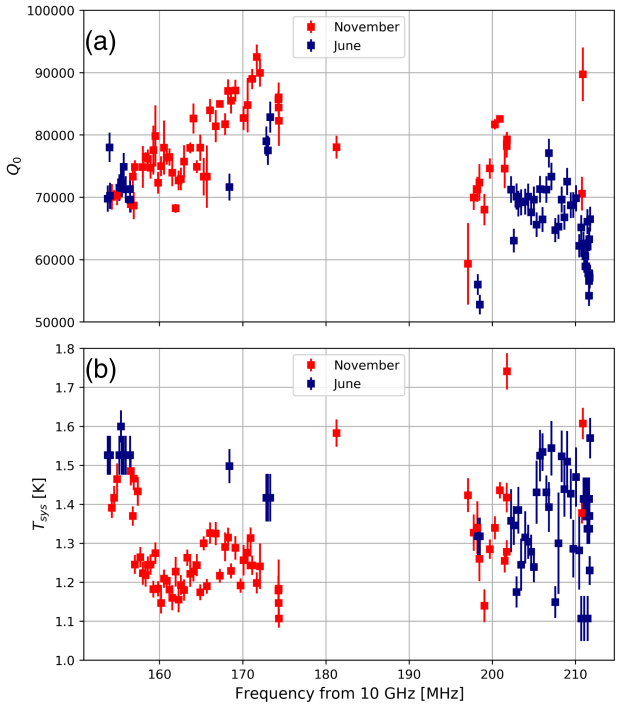

FIG. 3. System parameters for each frequency measurement point P_m. Blue (red) data markers are from June (November) session. (a) Unloaded cavity quality factor Q_0. Cavity resonance frequency f_c, coupling β, not shown in the figure, and quality factor Q_0 are derived from transmission and reflection measurements using a spectrum analyzer with a tracking generator. (b) System noise temperature values $T_{\rm sys}$.

110 s. The TWPA working parameters are optimized at every cavity frequency change: this optimization procedure is performed manually by setting the gain difference between having the pump driving the amplifier on or off above 25–26 dB. This level was very close to the TWPA gain saturation: in the first session we used to keep a higher margin with respect to saturation, while in the second session we reduced this margin since we noticed that the TWPA was stable enough to allow for long-lasting measurements. Since the added noise by the second stage amplifier is significant, higher TWPA gain resulted in lower values of $T_{\rm sys}$ [35]. The minimum observed $T_{\rm sys}$ was at about 1.1 K, corresponding to 2.3 photons [see Fig. 3(b)]. This is the lowest noise temperature obtained for a tunable haloscope working above 40 μeV [20,36,37].

The magnetic field is provided by a vertically aligned solenoidal coil of 450 mm length and 150 mm bore diameter. With a current of 92 A the magnet delivers a peak magnetic field of 8.0 T. The integrated value of B^2 over the cavity length is 50.2 T^2 m. A second coil reduces the stray field on sensitive electronics. Moreover, the TWPA is shielded from residual magnetic fields by using two encapsulated boxes of lead and μ metal.

As mentioned above, typical measurements at points P_m in axion search lasted about 1 h. Since the system was not

completely automated, such steps were performed during daily operation of the haloscope. During night operation, 8 h long data acquisitions were performed. Careful preliminary analysis of the collected data showed that in most cases the working parameters did not change significantly during acquisition and that the sensitivity scaled as expected; i.e., following Dicke's formula [38] with the square root of integration time. This is an important feature in case of positive alarms: longer integration time will increase the signal to noise ratio as envisaged.

Data analysis and results—Every saved file is divided in chunks of 2^{14} samples, corresponding to ∼4 ms duration: on each of these chunks the complex fast Fourier transform is performed, with a resulting bin width of $\Delta\nu_{\rm bin} \simeq 268$ Hz. These down-converted power spectra (PSD) span the actual range $[f_{\rm LO} - 2.2\ {\rm MHz},\ f_{\rm LO} + 2.2\ {\rm MHz}]$, with the cavity frequency belonging to the upper half of each spectrum.

Some preprocessing of the data is due. First, a systematic unwanted intruding power at the mixer level, coming from a defective grounding of the HEMT amplifier power supplies, is removed. Such a defect occasionally introduces an additional ∼4 mK of equivalent noise temperature power in two ∼50 kHz wide regions symmetrical with respect to $f_{\rm LO}$. The disturbance is symmetric about $f_{\rm LO}$ and is removed from the upper half of each PSD using lower half values.

The stability of the detection chain gain and of the cavity resonance frequency at each measurement P_m are checked. The former is estimated by injecting a low power pure tone in the detection chain at a frequency $f_{\rm ref} = f_{\rm LO} - 200$ kHz. The measured power at $f_{\rm ref}$, obtained for all blocks of 512 consecutive PSDs (about 1.9 s) of a specific P_m, is used to normalize all its PSDs. Another required normalization takes into account frequency-dependent contributions of the amplification chain, namely, the TWPA gain profile and the transmissivity of the ADC input filters.

The stability of the cavity resonance frequency can be checked by fitting the power spectra in a region around f_c with a Fano-like function [26,30]. This is performed on the average of 20×512 consecutive PSDs, corresponding to a 38 s time window. In case of variations of the resonance frequency above 20% of the cavity linewidth in a point P_m, varied data are moved to a new measurement point. This process increases the number of measured points to 147, each having a corresponding averaged spectrum, with proven constant cavity resonance frequency, quality factor, and antenna coupling.

For each averaged spectrum a frequency window of maximum three cavity linewidths inside the interval $[f_{\rm LO} + 0.5\ {\rm MHz}, f_{\rm LO} + 1.5\ {\rm MHz}]$ is selected. To recover the appropriate power units, the spectra are normalized, at the

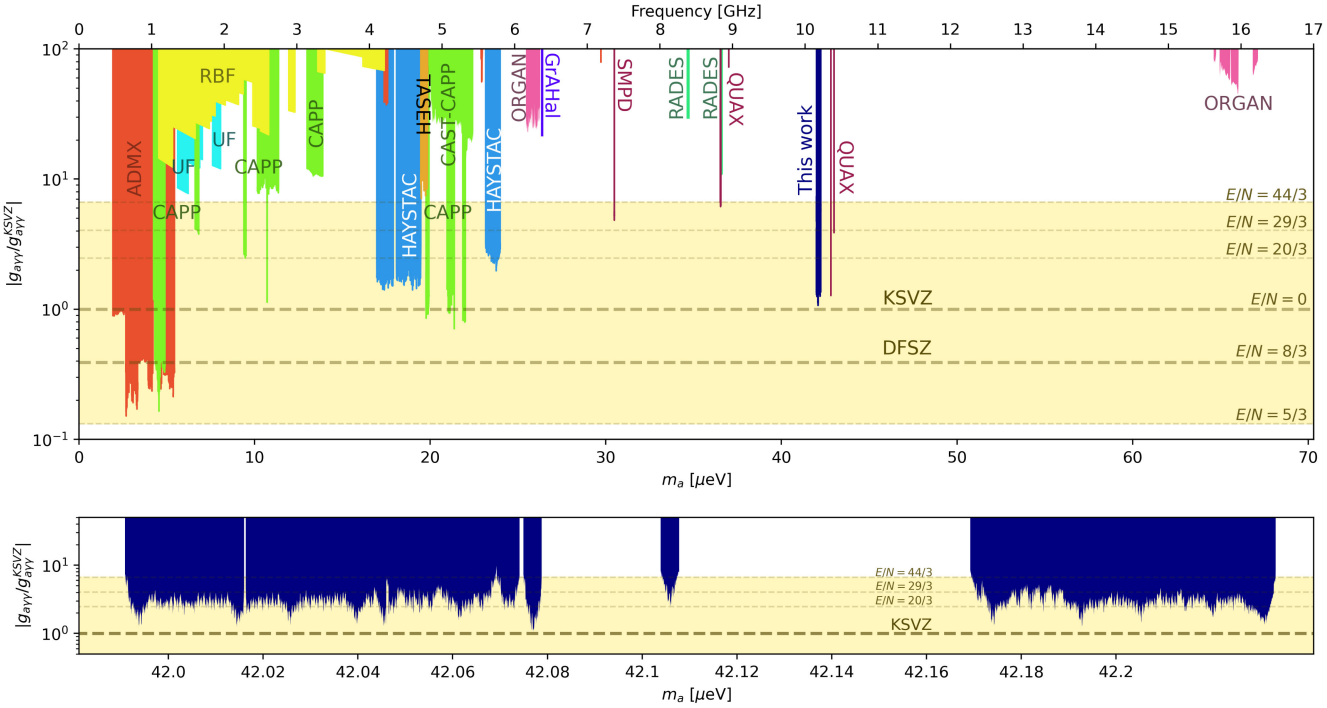

FIG. 4. Axion-photon coupling exclusion regions at 90% CL as a function of axion mass from this work, previous QUAX results [26–30] and other cavity haloscope searches: RBF [43,44], UF [45,46], ADMX [17,47–54], CAPP [18,55–64], HAYSTAC [19,65–68], TASEH [69], CAST-CAPP [70], RADES [71,72], ORGAN [37,73], and recent results using a single microwave photon detector (SMPD) [74]. The yellow band encloses the expected axion photon coupling as predicted in phenomenologically preferred models for which the anomaly coefficient ratio $E/N \in (5/3, 44/3)$ [75,76], generalization of the standard KSVZ model ($E/N = 0$) [8,9]. Lower panel shows the closeup of the results of this work, in order to better identify the exclusion region for the models with $E/N = 44/3$ and $29/3$. The missing band at about 42.017 μeV is due to data removal for rf contamination. Plot generated using [77].

cavity peak f_c, to the power given by the noise temperature, i.e., $k_B T_{\rm sys} \Delta\nu_{\rm bin}$, where k_B is the Boltzmann constant. The spectra are then divided by the Lorentzian cavity line shape to obtain an input noise spectrum $S_m(f)$ for each P_m, where it is possible to look for an added axion signal.

For each $S_m(f)$, a Savitzky-Golay (SG) filter, with polynomial order 4 and window range ∼110 kHz, is used to estimate the baseline $S_{\rm bl,m}(f)$. To search for axion excess power, confidence belts (CBs) are computed using Monte Carlo simulations. Axion signal power is given by

$$P^a_{\rm in}(\nu,\nu_a) = g^2_{a\gamma\gamma}\frac{\hbar^3 c^3 \rho_a}{m_a^2}\frac{2\pi\nu_a}{\mu_0} f_a(\nu,\nu_a), \qquad (1)$$

where $g_{a\gamma\gamma}$ is the coupling constant of the axion-photon interaction, $m_a = h\nu_a$ is the axion mass, $\rho_a \sim 0.45\ {\rm GeV/cm^3}$ is the local dark matter density [39] with Maxwell-Boltzmann distribution $f_a(\nu,\nu_a)$, characterized by a width $\delta_{\nu_a} \sim 10$ kHz in the Earth reference frame [40].

The entire measurement window is analyzed at the hypothetical frequencies ν_a^i, spaced by $\delta_{\nu_a}/2$. Assuming the Dicke radiometer equation and using as baseline $S_{\rm bl,m}(f) + k \cdot P^a_{\rm in}(\nu,\nu_a^i)$, 10 000 random spectra have been generated for each ν_a^i and all k. The values of k are chosen such that the signal to noise ratio (SNR) ranges from 0 to 10 at steps of 0.25. SNR = 1 occurs when $k \cdot P^a_{\rm in}(\nu,\nu_a^i)$ integrated in $I_a = [\nu_a^i, \nu_a^i + \delta_{\nu_a}]$ is equal to the variance of the noise in the same interval. The chosen interval is proven to maximize the SNR for the axion line shape in Eq. (1). Axion power is calculated using $g^{\rm KSVZ}_{a\gamma\gamma}(\nu_a \simeq 10.2\ {\rm GHz}) \simeq 1.67 \times 10^{-14}\ {\rm GeV^{-1}}$, the coupling constant of KSVZ model [8,9]. These data are used for the construction of the CBs after a baseline removal. Every CB is corrected to take into account the excess power non-negativity [41]. All the CBs show that the SG filtering is responsible for a ∼30% underestimation of the axion power [42].

In order to have an expected false alarm rate of one per month, the detection threshold is set to SNR = 4.5 using receiver operating characteristic curves. Since no rescan candidate is found, the PSDs are used to set a 90% confidence level (CL) limit on the coupling constant $g_{a\gamma\gamma}$ using Eq. (1). Figure 4 shows the resulting limits, which include the error budget for the measured cavity and receiver parameters, accounting on average about 4%. Hadronic axion models with anomaly coefficient ratio $E/N = 44/3$ ($E/N = 29/3$) are excluded in a mass interval of 153 neV (136 neV), located between 41.991 and 42.234 μeV [12]. As a global characterization of the apparatus, a 90% CL limit sensitivity of about $|g_{a\gamma\gamma}| \simeq 3.4 \times |g^{\rm KSVZ}_{a\gamma\gamma}|$ over a 300 kHz band is reached on average with an integration time of 1 h.

Conclusion and outlook—The scanning within a ∼60 MHz extended region with a sensitivity to axion-photon coupling up to the KSVZ class of models presented in this Letter is a significant advancement in the search for dark matter axions in the well motivated region $m_a \gtrsim 40$ μeV. This outcome relies on the use of a dielectrically loaded tunable cavity designed to have large effective volume even at high frequency, and on a quantum-limited, wide-bandwidth detection chain that we successfully operated in the presence of a strong magnetic field. Moving forward, the QUAX apparatus will be enhanced by a more powerful magnet, and in addition a duty cycle increase is foreseen, thus heading for better sensitivity and faster scan rate. This apparatus lays the foundations for a tunable QCD axion haloscope capable to cover the proposed frequency range from 9.5 to 11 GHz.

Acknowledgments—We are grateful to E. Berto, A. Benato, and M. Rebeschini for the mechanical work; F. Calaon and M. Tessaro for help with the electronics and cryogenics. We thank G. Galet and L. Castellani for the development of the magnet power supply, and M. Zago who realized the technical drawings of the system. We thank J. Pazzini, F. Fanzago, and A. Calanca for setting up the cloud data storage. We thank L. Di Luzio for support on hadronic axion models. We deeply acknowledge the Cryogenic Service of the Laboratori Nazionali di Legnaro for providing us with large quantities of liquid helium on demand. This work is supported by INFN (QUAX experiment), by the U.S. Department of Energy, Office of Science, National Quantum Information Science Research Centers, Superconducting Quantum Materials and Systems Center (SQMS) under Contract No. DE-AC02-07CH11359. Optimization of the TWPA amplifier was accomplished within the INFN project PNRR-ICSC Spoke 10.

Data availability—The data that support the findings of this article are not publicly available upon publication because it is not technically feasible and/or the cost of preparing, depositing, and hosting the data would be prohibitive within the terms of this research project. The data are available from the authors upon reasonable request.

[1] R. D. Peccei and H. R. Quinn, *CP* conservation in the presence of pseudoparticles, Phys. Rev. Lett. **38**, 1440 (1977).
[2] S. Weinberg, A new light boson?, Phys. Rev. Lett. **40**, 223 (1978).
[3] F. Wilczek, Problem of strong P and T invariance in the presence of instantons, Phys. Rev. Lett. **40**, 279 (1978).
[4] J. Preskill, M. B. Wise, and F. Wilczek, Cosmology of the invisible axion, Phys. Lett. **120B**, 127 (1983).
[5] L. F. Abbott and P. Sikivie, A cosmological bound on the invisible axion, Phys. Lett. **120B**, 133 (1983).
[6] M. Dine and W. Fischler, The not-so-harmless axion, Phys. Lett. **120B**, 137 (1983).
[7] I. G. Irastorza and J. Redondo, New experimental approaches in the search for axion-like particles, Prog. Part. Nucl. Phys. **102**, 89 (2018).

[8] J. E. Kim, Weak-interaction singlet and strong *CP* invariance, Phys. Rev. Lett. **43**, 103 (1979).

[9] M. A. Shifman, A. Vainshtein, and V. I. Zakharov, Can confinement ensure natural CP invariance of strong interactions?, Nucl. Phys. **B166**, 493 (1980).

[10] M. Dine, W. Fischler, and M. Srednicki, A simple solution to the strong CP problem with a harmless axion, Phys. Lett. **104B**, 199 (1981).

[11] A. Zhitnitskij, On possible suppression of the axion-hadron interactions, Yad. Fiz. **31**, 497 (1980).

[12] L. Di Luzio, M. Giannotti, E. Nardi, and L. Visinelli, The landscape of QCD axion models, Phys. Rep. **870**, 1 (2020).

[13] P. Sikivie, Experimental tests of the invisible axion, Phys. Rev. Lett. **51**, 1415 (1983); **52**, 695(E) (1984).

[14] P. Sikivie, Detection rates for "invisible" axion searches, Phys. Rev. D **32**, 2988 (1985); **36**, 974(E) (1987).

[15] R. Bradley, J. Clarke, D. Kinion, L. J. Rosenberg, K. van Bibber, S. Matsuki, M. Mück, and P. Sikivie, Microwave cavity searches for dark-matter axions, Rev. Mod. Phys. **75**, 777 (2003).

[16] Y. K. Semertzidis and S. Youn, Axion dark matter: How to see it?, Sci. Adv. **8**, eabm9928 (2022).

[17] C. Boutan *et al.* (ADMX Collaboration), Axion Dark Matter eXperiment: Run 1A analysis details, Phys. Rev. D **109**, 012009 (2024).

[18] S. Ahn *et al.*, Extensive search for axion dark matter over 1 GHz with CAPP's main axion experiment, Phys. Rev. X **14**, 031023 (2024).

[19] M. J. Jewell *et al.* (HAYSTAC Collaboration), New results from HAYSTAC's phase II operation with a squeezed state receiver, Phys. Rev. D **107**, 072007 (2023).

[20] G. Hoshino, S. Knirck, M. H. Awida, G. I. Cancelo, S. Corrodi, M. Di Federico, B. Knepper, A. Lapuente, M. Littmann, D. W. Miller, D. V. Mitchell, D. Rodriguez, M. K. Ruschman, C. P. Salemi, M. A. Sawtell, L. Stefanazzi, A. Sonnenschein, G. W. Teafoe, and P. Winter (GigaBREAD Collaboration), First axionlike particle results from a broadband search for wavelike dark matter in the 44 to 52 μeV range with a coaxial dish antenna, Phys. Rev. Lett. **134**, 171002 (2025).

[21] B. A. dos Santos Garcia *et al.*, First search for axion dark matter with a MADMAX prototype, Phys. Rev. Lett. **135**, 041001 (2025).

[22] A. J. Millar *et al.*, Searching for dark matter with plasma haloscopes, Phys. Rev. D **107**, 055013 (2023).

[23] M. Buschmann, J. W. Foster, A. Hook, A. Peterson, D. E. Willcox, W. Zhang, and B. R. Safdi, Dark matter from axion strings with adaptive mesh refinement, Nat. Commun. **13**, 1049 (2022).

[24] J. N. Benabou, M. Buschmann, J. W. Foster, and B. R. Safdi, Axion mass prediction from adaptive mesh refinement cosmological lattice simulations, Phys. Rev. Lett. **134**, 241003 (2025).

[25] C. A. J. O'Hare, G. Pierobon, J. Redondo, and Y. Y. Y. Wong, Simulations of axionlike particles in the postinflationary scenario, Phys. Rev. D **105**, 055025 (2022).

[26] A. Rettaroli *et al.* (QUAX Collaboration), Search for axion dark matter with the QUAX–LNF tunable haloscope, Phys. Rev. D **110**, 022008 (2024).

[27] D. Alesini *et al.*, Galactic axions search with a superconducting resonant cavity, Phys. Rev. D **99**, 101101(R) (2019).

[28] D. Alesini *et al.*, Search for invisible axion dark matter of mass $m_a = 43$ μeV with the QUAX–$a\gamma$ experiment, Phys. Rev. D **103**, 102004 (2021).

[29] D. Alesini *et al.*, Search for galactic axions with a high-q dielectric cavity, Phys. Rev. D **106**, 052007 (2022).

[30] R. Di Vora *et al.* (QUAX Collaboration), Search for galactic axions with a traveling wave parametric amplifier, Phys. Rev. D **108**, 062005 (2023).

[31] R. Di Vora, A. Gardikiotis, C. Braggio, G. Carugno, A. Lombardi, A. Ortolan, and G. Ruoso, A tunable dielectric-loaded copper resonator for axion searches at 11 GHz, Rev. Sci. Instrum. **96**, 085204 (2025).

[32] P. Sikivie, Invisible axion search methods, Rev. Mod. Phys. **93**, 015004 (2021).

[33] L. C. Maier Jr and J. Slater, Field strength measurements in resonant cavities, J. Appl. Phys. **23**, 68 (1952).

[34] A. Ranadive, M. Esposito, L. Planat, E. Bonet, C. Naud, O. Buisson, W. Guichard, and N. Roch, Kerr reversal in Josephson meta-material and traveling wave parametric amplification, Nat. Commun. **13**, 1737 (2022).

[35] C. Braggio, G. Cappelli, G. Carugno, N. Crescini, R. D. Vora, M. Esposito, A. Ortolan, L. Planat, A. Ranadive, N. Roch, and G. Ruoso, A haloscope amplification chain based on a traveling wave parametric amplifier, Rev. Sci. Instrum. **93**, 094701 (2022).

[36] R. Cervantes, G. Carosi, S. Kimes, C. Hanretty, B. H. LaRoque, G. Leum, P. Mohapatra, N. S. Oblath, R. Ottens, Y. Park, G. Rybka, J. Sinnis, and J. Yang, ADMX-Orpheus first search for 70 μeV dark photon dark matter: Detailed design, operations, and analysis, Phys. Rev. D **106**, 102002 (2022).

[37] A. Quiskamp, B. T. McAllister, P. Altin, E. N. Ivanov, M. Goryachev, and M. E. Tobar, Direct search for dark matter axions excluding ALP cogenesis in the 63- to 67-μeV range with the ORGAN experiment, Sci. Adv. **8**, eabq3765 (2022).

[38] R. H. Dicke, The measurement of thermal radiation at microwave frequencies, in *Classics in Radio Astronomy* (Springer, Dordrecht, 1946), pp. 106–113.

[39] P. A. Zyla *et al.* (Particle Data Group), Review of particle physics, Prog. Theor. Exp. Phys. **2020**, 083C01 (2020).

[40] M. S. Turner, Periodic signatures for the detection of cosmic axions, Phys. Rev. D **42**, 3572 (1990).

[41] G. J. Feldman and R. D. Cousins, Unified approach to the classical statistical analysis of small signals, Phys. Rev. D **57**, 3873 (1998).

[42] A. Gallo Rosso, J. Conrad, and J. Jeong, Baseline filtering and peak reconstruction for haloscope-like axion searches, J. High Energy Phys. 07 (2025) 191.

[43] S. DePanfilis, A. C. Melissinos, B. E. Moskowitz, J. T. Rogers, Y. K. Semertzidis, W. U. Wuensch, H. J. Halama, A. G. Prodell, W. B. Fowler, and F. A. Nezrick, Limits on the abundance and coupling of cosmic axions at $4.5 < m_a < 5.0 \times$ μeV, Phys. Rev. Lett. **59**, 839 (1987).

[44] W. U. Wuensch, S. De Panfilis-Wuensch, Y. K. Semertzidis, J. T. Rogers, A. C. Melissinos, H. J. Halama, B. E. Moskowitz, A. G. Prodell, W. B. Fowler, and F. A. Nezrick, Results of a laboratory search for cosmic axions and other weakly coupled light particles, Phys. Rev. D **40**, 3153 (1989).

[45] C. Hagmann, P. Sikivie, N. S. Sullivan, and D. B. Tanner, Results from a search for cosmic axions, Phys. Rev. D **42**, 1297 (1990).
[46] C. Hagmann, D. Kinion, W. Stoeffl, K. van Bibber, E. Daw, J. McBride, H. Peng, L. Rosenberg, H. Xin, J. Laveigne, P. Sikivie, N. Sullivan, D. Tanner, D. Moltz, F. Nezrick, M. Turner, N. Golubev, and L. Kravchuk, First results from a second generation galactic axion experiment, Nucl. Phys. B, Proc. Suppl. **51**, 209 (1996).
[47] S. J. Asztalos, G. Carosi, C. Hagmann, D. Kinion, K. van Bibber, M. Hotz, L. J. Rosenberg, G. Rybka, J. Hoskins, J. Hwang, P. Sikivie, D. B. Tanner, R. Bradley, and J. Clarke, Squid-based microwave cavity search for dark-matter axions, Phys. Rev. Lett. **104**, 041301 (2010).
[48] N. Du *et al.* (ADMX Collaboration), Search for invisible axion dark matter with the axion dark matter experiment, Phys. Rev. Lett. **120**, 151301 (2018).
[49] T. Braine *et al.* (ADMX Collaboration), Extended search for the invisible axion with the axion dark matter experiment, Phys. Rev. Lett. **124**, 101303 (2020).
[50] C. Bartram *et al.* (ADMX Collaboration), Search for invisible axion dark matter in the $3.3 - 4.2$ μeV mass range, Phys. Rev. Lett. **127**, 261803 (2021).
[51] C. Boutan *et al.* (ADMX Collaboration), Piezoelectrically tuned multimode cavity search for axion dark matter, Phys. Rev. Lett. **121**, 261302 (2018).
[52] C. Goodman *et al.* (ADMX Collaboration), ADMX axion dark matter bounds around 3.3 μeV with Dine-Fischler-Srednicki-Zhitnitsky discovery ability, Phys. Rev. Lett. **134**, 111002 (2025).
[53] C. Bartram *et al.*, Dark matter axion search using a Josephson traveling wave parametric amplifier, Rev. Sci. Instrum. **94**, 044703 (2023).
[54] G. Carosi, C. Cisneros, N. Du, S. Durham, N. Robertson, C. Goodman, M. Guzzetti, C. Hanretty, K. Enzian, L. Rosenberg *et al.*, Search for axion dark matter from 1.1 to 1.3 GHz with ADMX, Phys. Rev. Lett. **135**, 191001 (2025).
[55] S. Lee, S. Ahn, J. Choi, B. R. Ko, and Y. K. Semertzidis, Axion dark matter search around 6.7 μeV, Phys. Rev. Lett. **124**, 101802 (2020).
[56] J. Jeong, S. W. Youn, S. Bae, J. Kim, T. Seong, J. E. Kim, and Y. K. Semertzidis, Search for invisible axion dark matter with a multiple-cell haloscope, Phys. Rev. Lett. **125**, 221302 (2020).
[57] O. Kwon *et al.*, First results from an axion haloscope at CAPP around 10.7 μeV, Phys. Rev. Lett. **126**, 191802 (2021).
[58] Y. Lee, B. Yang, H. Yoon, M. Ahn, H. Park, B. Min, D. L. Kim, and J. Yoo, Searching for invisible axion dark matter with an 18 T magnet haloscope, Phys. Rev. Lett. **128**, 241805 (2022).
[59] H. Yoon, M. Ahn, B. Yang, Y. Lee, D. L. Kim, H. Park, B. Min, and J. Yoo, Axion haloscope using an 18 T high temperature superconducting magnet, Phys. Rev. D **106**, 092007 (2022).
[60] J. Kim, O. Kwon, i. m. c. b. u. Kutlu, W. Chung, A. Matlashov, S. Uchaikin, A. F. van Loo, Y. Nakamura, S. Oh, H. Byun, D. Ahn, and Y. K. Semertzidis, Near-quantum-noise axion dark matter search at CAPP around 9.5 μeV, Phys. Rev. Lett. **130**, 091602 (2023).
[61] A. K. Yi *et al.*, Axion dark matter search around 4.55 μeV with Dine-Fischler-Srednicki-Zhitnitskii sensitivity, Phys. Rev. Lett. **130**, 071002 (2023).
[62] B. Yang, H. Yoon, M. Ahn, Y. Lee, and J. Yoo, Extended axion dark matter search using the CAPP18T haloscope, Phys. Rev. Lett. **131**, 081801 (2023).
[63] Y. Kim, J. Jeong, S. W. Youn, S. Bae, K. Lee, A. F. van Loo, Y. Nakamura, S. Oh, T. Seong, S. Uchaikin, J. E. Kim, and Y. K. Semertzidis, Experimental search for invisible dark matter axions around 22 μeV, Phys. Rev. Lett. **133**, 051802 (2024).
[64] S. Bae, J. Jeong, Y. Kim, S. W. Youn, J. Kim, A. F. van Loo, Y. Nakamura, S. Oh, T. Seong, S. Uchaikin, J. E. Kim, and Y. K. Semertzidis, Axion dark matter search with sensitivity near the Kim-Shifman-Vainshtein-Zakharov benchmark using the TM_{020} mode, Phys. Rev. Lett. **135**, 091804 (2025).
[65] B. M. Brubaker *et al.*, First results from a microwave cavity axion search at 24 μeV, Phys. Rev. Lett. **118**, 061302 (2017).
[66] K. M. Backes *et al.*, A quantum enhanced search for dark matter axions, Nature (London) **590**, 238 (2021).
[67] L. Zhong *et al.*, Results from phase 1 of the HAYSTAC microwave cavity axion experiment, Phys. Rev. D **97**, 092001 (2018).
[68] X. Bai *et al.* (HAYSTAC Collaboration), Dark matter axion search with HAYSTAC phase II, Phys. Rev. Lett. **134**, 151006 (2025).
[69] H. Chang, J.-Y. Chang, Y.-C. Chang, Y.-H. Chang, Y.-H. Chang, C.-H. Chen, C.-F. Chen, K.-Y. Chen, Y.-F. Chen, W.-Y. Chiang, W.-C. Chien, H. T. Doan, W.-C. Hung, W. Kuo, S.-B. Lai, H.-W. Liu, M.-W. OuYang, Ping-I. Wu, and S.-S. Yu, First results from the Taiwan axion search experiment with a haloscope at 19.6 μeV, Phys. Rev. Lett. **129**, 111802 (2022).
[70] C. M. Adair *et al.*, Search for dark matter axions with CAST-CAPP, Nat. Commun. **13**, 6180 (2022).
[71] A. Álvarez Melcón *et al.*, First results of the CAST-RADES haloscope search for axions at 34.67 μeV, J. High Energy Phys. 10 (2021) 075.
[72] S. Ahyoune, A. Á. Melcón, S. A. Cuendis, S. Calatroni, C. Cogollos, A. Díaz-Morcillo, B. Döbrich, J. Gallego, J. García-Barceló, B. Gimeno *et al.*, Rades axion search results with a high-temperature superconducting cavity in an 11.7 T magnet, J. High Energy Phys. 04 (2025) 113.
[73] A. P. Quiskamp, G. R. Flower, S. Samuels, B. T. McAllister, P. Altin, E. N. Ivanov, M. Goryachev, and M. E. Tobar, Near-quantum-limited axion dark matter search with the organ experiment around 26 μeV, Phys. Rev. D **111**, 095007 (2025).
[74] C. Braggio, L. Balembois, R. Di Vora, Z. Wang, J. Travesedo, L. Pallegoix, G. Carugno, A. Ortolan, G. Ruoso, U. Gambardella, D. D'Agostino, P. Bertet, and E. Flurin, Quantum-enhanced sensing of axion dark matter with a transmon-based single microwave photon counter, Phys. Rev. X **15**, 021031 (2025).
[75] L. Di Luzio, F. Mescia, and E. Nardi, Redefining the axion window, Phys. Rev. Lett. **118**, 031801 (2017).
[76] L. Di Luzio, F. Mescia, and E. Nardi, Window for preferred axion models, Phys. Rev. D **96**, 075003 (2017).
[77] C. O'Hare, cajohare/AxionLimits: AxionLimits, https://cajohare.github.io/AxionLimits/ (2020).